Desalination and Water Treatment
www.deswater.com

doi: 10.5004/dwt.2022.28590

262 (2022) 266–282
June

Kinetic and adsorption isotherm modeling of photodegradation of anionic dyes using polyazomethine/titanium dioxide and polyazomethine/zinc oxide nanocomposite

S.J. Pradeeba[a,*], K. Sampath[b], B. Jeyagowri[a]

[a]*Department of Chemistry, Hindusthan College of Engineering and Technology, Coimbatore, Tamil Nadu, India, email: pradeebasj@gmail.com (S.J. Pradeeba)*
[b]*Department of Chemistry, Kumaraguru College of Technology, Coimbatore, Tamil Nadu, India*

Received 23 January 2022; Accepted 19 May 2022

ABSTRACT

Poly(azomethine), ZnO, TiO_2, poly(azomethine)/TiO_2, and poly(azomethine)/ZnO nanocomposites were synthesized and structural characterization were studied using Fourier-transform infrared spectroscopy, UV-Visible spectroscopy, powder X-ray diffraction, energy-dispersive X-ray spectroscopy (EDAX), and scanning electron microscopy (SEM). Photocatalytic experiment was carried out by varying dye concentrations from 10 to 50 ppm using synthesized photocatalyst in presence of natural sunlight. The degradation efficiency, reaction kinetics, and isotherm studies revealed that the poly(azomethine) PAZ/ZnO (PNZ) nanocomposites have excellent photocatalytic activity than PAZ, ZnO, TiO_2, and poly(azomethine)/TiO_2 (PNT). At optimum dye concentrations of 10 ppm methyl orange and Alizarin Red S shows maximum degradation efficiency was 87% and 86% using PAZ/ZnO nanocomposites, as a photocatalysts. The maximum time that required for the dye to degrade was 5 h. Fourier-transform infrared spectroscopy UV-Visible spectroscopy, SEM, and EDAX were used to describe the samples after the photocatalytic investigation. To examine the effect of decolorisation of dyes using synthesised photocatalysts pseudo-first-order kinetic, pseudo-second-order model, Langmuir and Freundlich isotherms studies were carried out. This can be a step or an economical social measure to get into a generation which effectively uses the available resources for the essential human needs rather than creating a system which can destruct the environment sooner or later causing chaos to the future generation.

Keywords: Polyazomethine; Photocatalyst; Nanocomposites; Anionic dyes; Kinetic model; Degradation efficiency

1. Introduction

Water plays a significant role in the global economy. About 70% of the clean water used by an individual is for cultivation. Fishing in salt and fresh water bodies is an important source of food for people in numerous parts of the world. To a great extent of long-distance trade of supplies (such as oil and natural gas) and artificial products is transported by boats through seas, rivers, lakes, and canals. Huge amount of water, ice, and steam are used for cooling and heating, in industry and homes. Water is an admirable solvent for a large diversity of chemical stuffs; as such it is generally used in industrial development, and in cooking and washing. Water is also essential to various sports and other forms of activity such as swimming, pleasure boating, boat racing, surfing, sport fishing, and diving.

Nowadays pollution due to dyes discharge in water becomes major threat to human beings. Dyes and pigment removal from wastewater has been a prominent research focused currently. Since the existence of dyes and pigments

* Corresponding author.

in water, even at very low concentrations, is extremely disagreeable. The sum of yearly manufacturing of dyes globally is higher than 7×10^5 tons and about 2% of dyes produced per annum are released in waste matter from industrialized process. India has become a prominent producer of dyes and pigments for the past 35 y, other than textiles industries, it is used for printing inks, plastics, rubber, paints, paper, art and craft, cosmetics, leather, food, and pharmaceuticals. The release of dye waste materials into the atmosphere is today one of the world's most important environmental challenges in the point of the ecological reasons [1–9].

Acidic dyes are anionic dyes which are water soluble and used in textile cloth such as silk, wool, and nylon. Basic dyes are cationic dyes which are dissolved in water and used mostly on acrylic fabrics. Dyestuffs liberated from textile industries are the major organic chemicals that can pollute standing, flowing, and subsurface water system leads to a severe environmental threat. Biological, adsorption, degradation, ozonation, and chlorination are the most used approaches, however they are insufficient to remove these harmful chemicals from effluent discharged water streams [10–13].

Recently advanced oxidation processes was the major cost-effective treatment approach for eliminating dyes from industrial wastewater. However, the chemicals employed in dye manufacturing are frequently poisonous, carcinogenic, or unstable. As a result, they are unsuitable from an ecological perspective [1–5]. Even though advanced oxidation has been shown to be a successful method of treating industrial wastewater discharge, heterogeneous photocatalysis process revealed that it was most promising methods in removal of organic pollutants completely.

Among the various dyestuffs discharge from textile industries, methyl orange (MO) is a commonly used monoazo dye in laboratory assays, textiles and other commercial products and has to be removed from water due to its toxicity. Frequent exposure to methyl orange leads to gastrointestinal issues such as nausea, vomiting, and diarrhoea. Other issues include skin inflammation and eye irritation. In human being, there were a few symptoms of epidermal sensitization. Depending on the pH of the water, the Alizarin Red S dye generates a 'red' or 'purple' coloured solution. Physical, biological, and chemical treatments are three types of traditional procedures for removing dyeing effluents from aqueous solutions. Also it decrease light penetration and prevent photosynthesis when it is discharged in streams and lakes. Alizarin Red S is broadly used in the dyeing industry and causes frequent ecological problems [30].

Because of its increased photocatalytic property, high strength, and lack of toxicity, TiO_2 is the most widely used semiconductor as a photocatalyst. ZnO is a high-quality semiconductor material with a same energy band gap like TiO_2, and it has revealed to be more efficient than TiO_2 in photocatalytic process. In the presence of sunlight, however, the reaction rate is low due to rapid rejoining of charge carriers, and the use of ZnO is limited to some extent due to the significant disadvantage of photo corrosion. To overcome these drawbacks, an attempt have been made to avoid the recombining of photogenerated hole/electron pairs and to enhance the effectiveness of solar radiation in photocatalytic reactions through external rearrangement, which can be accomplished through alloying, doping, or the combination of narrow band gap semiconductors [29].

Poly(azomethine)s or Schiff bases or conjugated polymers, suggest a broad range of usage in electronics, optoelectronics, and photonics, and are particularly appealing because of their structure-function relationship [30]. Many challenges have been made in the past to remove dyestuffs using polymer metal oxide nanocomposites with higher photocatalytic activity, some of which are listed in Table 1.

Based on the above literature survey, present work was carried out using poly(azomethine) PAZ, TiO_2, ZnO, PAZ/TiO_2 (PNT), PAZ/ZnO (PNZ) nanocomposites and structural characterization techniques such as Fourier-transform infrared spectroscopy (FTIR), UV-Vis, scanning electron microscopy (SEM), X-ray diffraction (XRD), and energy-dispersive X-ray spectroscopy (EDAX) was done. In the presence of natural sunlight, photocatalytic tests with poly(azomethine) PAZ/TiO_2 (PNT) and PAZ/ZnO (PNZ) nanocomposites were carried out for the removal of methyl orange (MO) and Alizarin Red S (ARS) existing in waste water. Photocatalyst deprivation efficiency was measured and a graph was plotted.

2. Materials and methods

2.1. Synthesis of poly(azomethine)

The polymer synthesis is based on the reference work carried out by Vasanthi and Ravikumar [24]. About 0.5 mol of 4,4′-diformyl biphenyl monomer is taken in DMF medium added slowly into a mixture of toluene solution of 0.5 mol *p*-phenylenediamine. The contents of the reaction were refluxed for 6 h and then allowed to cool before being discharged into methanol. The resultant precipitate was filtered and dried (Fig. 1).

2.2. Synthesis of ZnO nanoparticle

Under vigorous stirring, an aqueous solution of KOH (0.4 M) is gradually discharged into a zinc nitrate solution (0.2 M) at room temperature, resulting in the formation of a white suspension. After being rinsed three times with filtered water, the whitish substance was centrifuged. The finished product was then cleaned in pure alcohol before being calcined at 500°C for 3 h.

2.3. Synthesis of TiO_2 nanoparticle

In an ice bath, $TiCl_4$ was gradually added to clean water with stirring until it was entirely dissolved simultaneously add NH_4OH (30%) solution was added. After 1 h, the white TiO_2 nanoparticle was filtered. Obtained TiO_2 nanoparticles were washed in clean water and dehydrated for 3 h under vacuum at 100°C.

2.4. Synthesis of ZnO/TiO_2 incorporated polyazomethine polymeric nanocomposite

500 mg polyazomethine is dissolved in 100 mL DMF solution and sonicated for 48 h under constant stirring. Under sonication, ZnO or TiO_2 nanoparticles are liberated

Table 1
List of few polymer metal oxide nanocomposites as photocatalysts and their efficiency reported in previous literature

Photocatalysts	Dyes removed	Degradation efficiency (%)	Reaction time and radiation source
Polyaniline/TiO_2 (PANI-TiO_2)	Metronidazole	98%	1 h UV and visible radiation [4]
Polyacrylamide (PAM)/TiO_2	Methyl orange	88%	5 h UV and visible radiation [5]
Poly(3-hexylthiophene)/titanium dioxide	Methyl orange	86%	1.5 h UV and visible light irradiation [6]
Polythiophene/titanium dioxide (PTh/TiO_2) composite	Rhodamine B	70%	3 h UV-Vis light irradiation [7]
PANI/ZnO	Methylene blue and malachite green	99%	5 h natural sunlight and UV light irradiation [8]
Poly(*m*-phenylenediamine)/ZnO	C.I. Acid Red	94.6%	3 h UV-Vis light irradiation [9]
Polyaniline PANI/CdO	Methylene blue and malachite green	99%	5 h UV light irradiation [10]
Poly(3,4-propylenedioxy-2,2′:5′, 2″-terthiophene)/TiO_2	Methylene blue	90.5%	3 h UV light and sunlight irradiation [11]
Poly(3,4-ethylenedioxythiophene)/zinc oxide	Methylene blue	96%	3 h UV light and sunlight irradiation [12]
Poly(3,4-ethylenedioxythiophene) (PEDOT)/ZnO	Reactive Red 45	91%	1.5 h simulated solar irradiation [13]
Polythiophene/TiO_2	Methyl orange	88.5%	3 h UV-Vis light irradiation [14]
Polyaniline (PANI)-based nanocomposites-doped with $SrTiO_3$ nanocubes	Methylene blue dye	90%	90 min visible light irradiation [15]
Polydopamine/TiO_2	Methylene blue	98%	3 h in visible light [16]
Chitosan-*g*-poly(acrylamide)/ZnS	Methyl orange (MO) and congo red (CR)	75% of congo red; 69% of methyl orange	4 h of simulated solar irradiation [17]
Phthalocyanine sensitized titanium dioxide (Pc/TiO_2)	Malachite green	90.3%	6 h in visible light [18]
Polythiophene/TiO_2	Methyl orange	95%	2 h UV-Visible light radiation [19]
Poly(*o*-phenylenediamine) modified TiO_2 nanocomposites	Methylene blue	98.3%	2 h visible light irradiation [20]
Polypyrrole-TiO_2 nanocomposite	Methylene blue	93%	2 h simulated solar light irradiation [21]
Gelatin/CuS/PVA nanocomposite	Rhodamine B	80%	1.5 h solar light irradiation [22]
H_2O_2/$NiFe_2O_4$	Methylene blue	99%	3 h visible light [23]

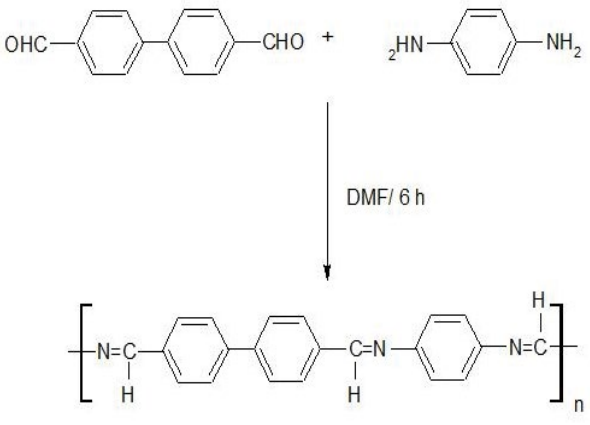

Fig. 1. Synthesis of polyazomethine (PAZ).

in acetone and simultaneously added to the polymeric solution. The precipitated ZnO incorporated polyazomethine (PNZ) or TiO_2 incorporated polyazomethine (PNT) composite material is filtered, washed repeatedly in acetone and dried out (Fig. 2) [24]. FTIR spectroscopy, UV-Vis spectroscopy, scanning electron microscopy, transmission electron microscopy and energy dispersive analysis X-ray powder X-ray diffraction were used to verify the synthesised polyazomethines (PNT and PNZ) [25–31].

2.5. Photocatalytic experiment

In the presence of a natural sunlight, batch mode photocatalytic investigations were carried out for the effective degradation of MO and ARS synthetic dyes utilising synthesised photocatalysts (PAZ, PNT, PNZ, TiO_2, and ZnO). Prior to irradiation, the suspension (50 mL dye

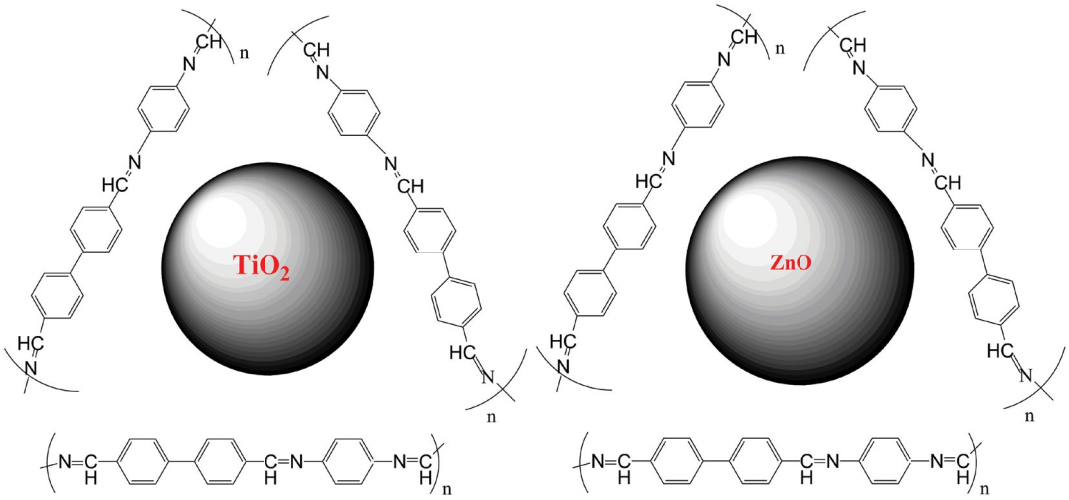

Fig. 2. Structure of PNT and PNZ nanocomposite.

solution + 20 mg photocatalyst) is stirred for 30 min with a magnetic stirrer (300 rpm) until adsorption–desorption equilibrium is reached. To attain effective photodegradation, the suspension was kept in natural sunlight irradiation after reaching adsorption–desorption equilibrium. A UV-Visible spectrophotometer was used to measure the absorbance of the dye solution, which was pipetted out once at periodic intervals. The photo deprivation efficacy $R(\%)$ was calculated using the Eq. (4):

$$R(\%) = \frac{C_0 - C_t}{C_0} \quad (1)$$

where C_0 symbolizes the dye concentration before irradiation and C_t indicates the dye concentration after a set period of time.

2.5.1. Effect of initial dye concentration

50 mL of MO and ARS dyes with concentrations of 10, 20, 30, 40, and 50 ppm were utilised to analysis the effect of initial dye concentration in optimized pH conditions for the time period of 1–5 h with 100 mg of synthesized photocatalysts (PAZ, TiO_2, ZnO, PNT and PNZ,).

3. Results and discussion

3.1. Characterization of photocatalyst

3.1.1. Fourier-transform infrared spectroscopy

The FTIR spectrum of synthetic photocatalysts is discussed in Table 2. There is no significant change in FTIR spectra after photodegradation. Minor changes in the peaks are caused by the absorption of methyl orange and Alizarin Red S (Fig. 3).

3.1.2. UV-Visible spectroscopy

In the tabular column below, the UV-Vis spectrum of synthesised photocatalysts is shown in Table 3.

Table 2
List of FTIR bands and related group presence in photocatalysts

Wavenumber (cm^{-1})	Group presence
1,512	Azomethine linkage (–CH–N)
3,736	N–H stretching vibration
3,555	C–H stretching in aromatic ring
1,387 and 1,352	C=C stretching in benzene ring
500–600	Stretching vibration frequency of TiO_2 and ZnO
1,629	H–O–H bending vibration
2,863	C–H bond
2,924 and 2,843	C–H stretching vibration of the alkane groups

The peak intensity was higher (Fig. 4), indicating the presence of auxochrome groups such as $–NH_2$ and –O in the structure. As a result, visible light or existing natural sunlight illumination can be used to photo-stimulate the produced nanocomposite, which has no harmful effects on human health [31–34].

After the photocatalytic process, the UV-Vis spectra of photocatalysts were studied. The absorption band in the visible region between 400 nm and 700 nm is caused by the removal of methyl orange and Alizarin Red S dye present in water [11,12].

3.1.3. X-ray diffraction

The XRD characterization studies of synthesized photocatalysts materials were explained in the below tabular column (Table 4).

The XRD pattern of ZnO the peaks are present in polyazomethine matrix and confirm the formation of PNZ nanocomposite (Fig. 5).

The XRD model of TiO_2 depicts diffraction peaks at 2θ values of 26.27, 31.80, 36.31, 42.04, 47.24, 52.28, 57.82, 62.23, 67.89 and 73.23 which might be assigned to the anatase

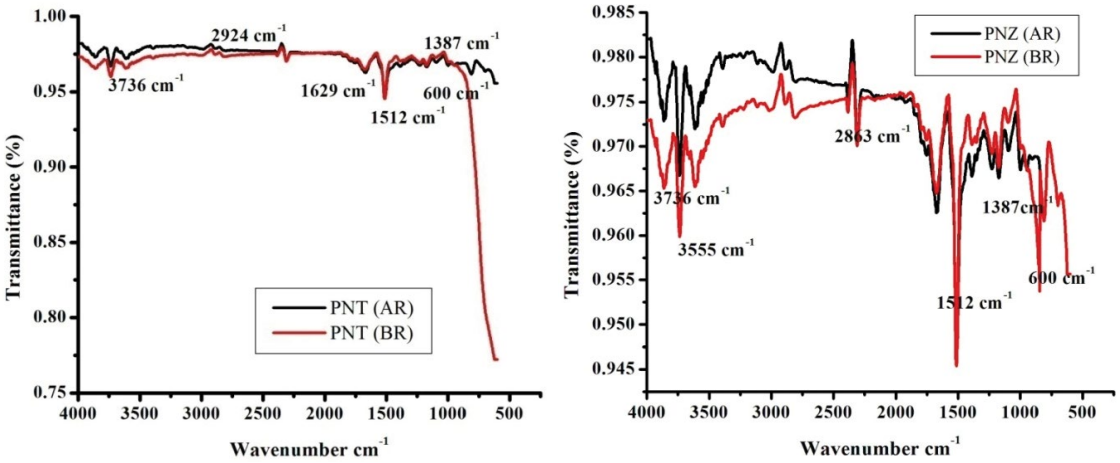

Fig. 3. Fourier-transform infrared spectrum of PNT and PNZ nanocomposite before (BR) and after (AR) elimination of anionic dyes.

Table 3
List of UV-Vis bands and related group presence in photocatalysts

Wavelength (nm)	Group presence
400–460	π–π* and n–π* transition between the benzenoid segments
490–500	Electron move from valence band
510–700	to the antibonding π–π* type of PAZ
215–280	TiO_2 nanoparticle
375	ZnO nanoparticle

Table 4
List of XRD peaks and element present in photocatalysts

2θ values	Interpretation
Sharp narrow peaks in PAZ	Recommend the material is crystalline with a little amorphous component
26.27, 31.80, 36.31, 42.04, 47.24, 52.28, 57.82, 62.23, 67.89, 73.23	Anatase phase TiO_2
29.21, 35.27, 40.08, 44.27, 49.09, 58.19, 63.67, 70.40	ZnO with hexagonal crystal structure

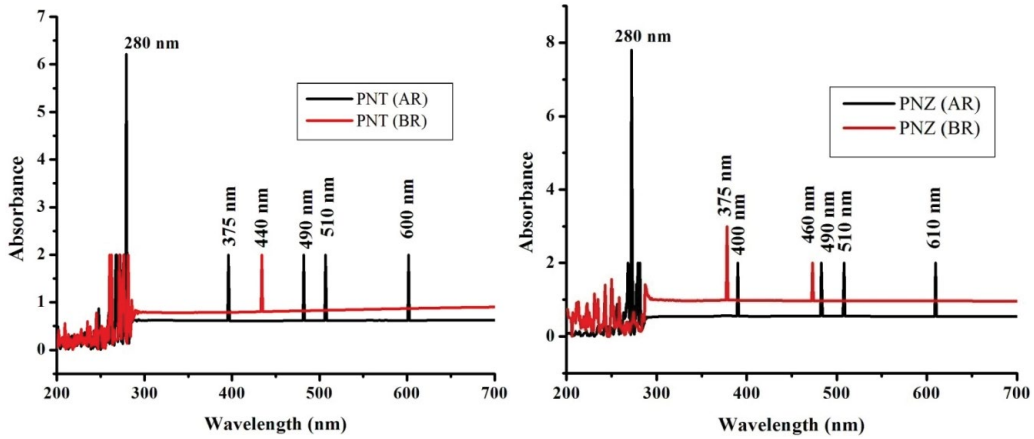

Fig. 4. Ultraviolet visible spectrum of PNT and PNZ nanocomposite before (BR) and after (AR) elimination of dyes.

phase in the TiO_2 (JCPDS-87-0598) [5]. The same peaks are present in polyazomethine matrix and confirm the formation of PNZ nanocomposite (Fig. 5). The particle size of photocatalysts synthesized was listed in the Table 5.

After study there is no change in XRD pattern (Fig. 5) of PNT and PNZ nanocomposite shows the stability of the synthesized photocatalyst.

From the Tauc plot of $\alpha h\nu$ (eV^2 m^{-2}) against photon energy (eV) the band gap energy of PAZ, TiO_2, ZnO, PNT and PNZ were calculated (Table 6)

It was observed that the calculated band gap energy of PNT and PNZ was found to be 2.89 and 2.9 eV respectively which was lower than the corresponding TiO_2 and ZnO nanoparticles calculated band gap 2.96 and 2.94 eV.

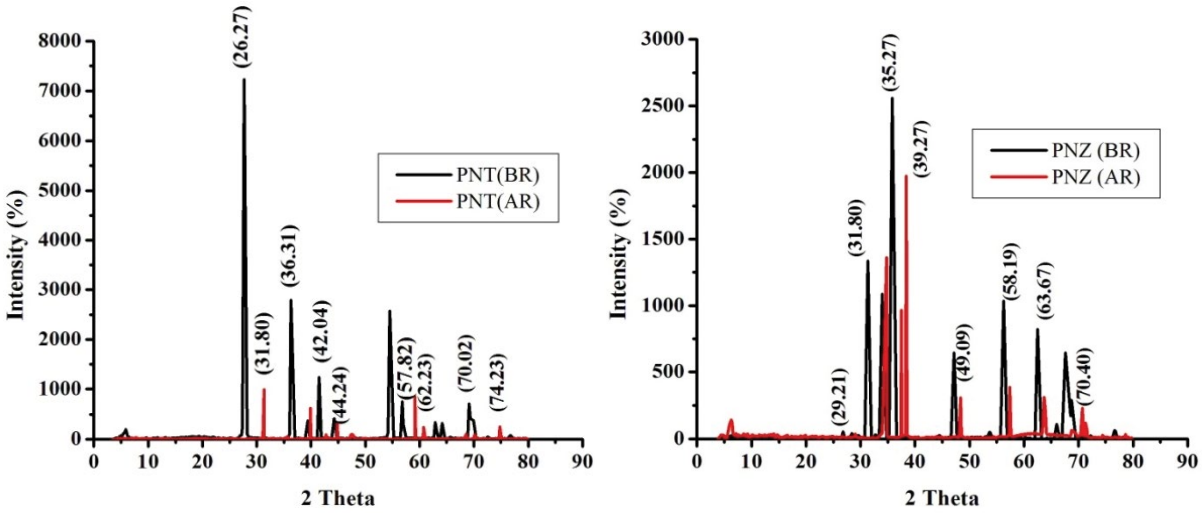

Fig. 5. X-ray diffraction peaks of PNT and PNZ nanocomposite before (BR) and after (AR) elimination of dyes.

Table 5
List of photocatalysts and their particle size

Photocatalysts	Particle size (nm)
PAZ	65
TiO_2	29
ZnO	32
PNT	30
PNZ	33.5

Table 6
Calculated band gap energy of the synthesized materials used for dye degradation

Synthesized materials	Wavelength (nm)	Band gap (eV)
PAZ (azomethine polymer)	530	2.93
TiO_2 nanoparticles	380	2.96
ZnO nanoparticles	483	2.94
PNT (polymeric nanocomposite)	665	2.89
PNZ (polymeric nanocomposite)	760	2.9

Therefore, addition of PAZ polymer onto TiO_2 and ZnO matrix resulted in the red shift in the wavelength of the adsorption to visible region. This shift makes it possible to carry out the photodegradation of dye molecules in the presence of sunlight proving to as visibly active photocatalyst. It showed that the photoabsorption of the photocatalyst depends on the mobility of electron–hole pairs, which determines the probability of electrons and holes to reach reaction sites of the photocatalyst surface.

3.1.4. Morphological studies

The SEM and EDAX image of PNT and PNZ nanoparticles before and after photocatalytic study have been examined which is represented in Figs. 6–8.

The SEM image (Fig. 8) confirms the adsorption of dye molecules on the surface of the photocatalysts. After degradation, changes in the elemental composition and the presence of new elements were found in the EDAX spectrum (Figs. 6 and 7) which confirms the dyestuffs adsorbed on the catalysts surface [35].

3.2. Synthesized composite materials photocatalytic activity in the existence of natural sunlight

Batch photocatalytic studies were carried out to determine the effect of variation of initial concentration on the effective removal of MO and ARS at a given dosage of photocatalysts at 100 mg at time interval between 1 to 5 h [9–11]. An increased amount of photocatalyst ranging from 10 to 50 ppm was used to determine the optimum dye concentration for removing MO and ARS.

The exponential variation of the percentage removal of dyes (MO and ARS) with the dose of catalysts (PAZ, TiO_2, ZnO, PNT and PNZ) is depicted in Figs. 9–14.

The results reveal that when the initial dye concentration increases, the degrading effectiveness of MO and ARS decreases. As the initial concentration of a dye solution rises, less light may reach the catalyst's surface, resulting in a decrease in the dye molecules activation [36,37].

The maximum degradation efficiency of MO and ARS at 5 h was depicted in the Table 7 and it was represented in Figs. 9–14. The order of degradation efficiency of photocatalysts in removal of dyes was as follows,

$$PNZ > PNT > ZnO > TiO_2 > PAZ \quad (2)$$

The maximum degradation efficiency percentage reached to 87% in the removal of MO and 86% in the removal of ARS. From these studies, optimum dye was found to be 10 ppm. In comparison to ZnO, TiO_2, PAZ, the PNZ and PNT nanocomposite shows an efficient photocatalyst material.

The degradation efficiency was compared with few photocatalyst materials listed in the Table 1. Since the

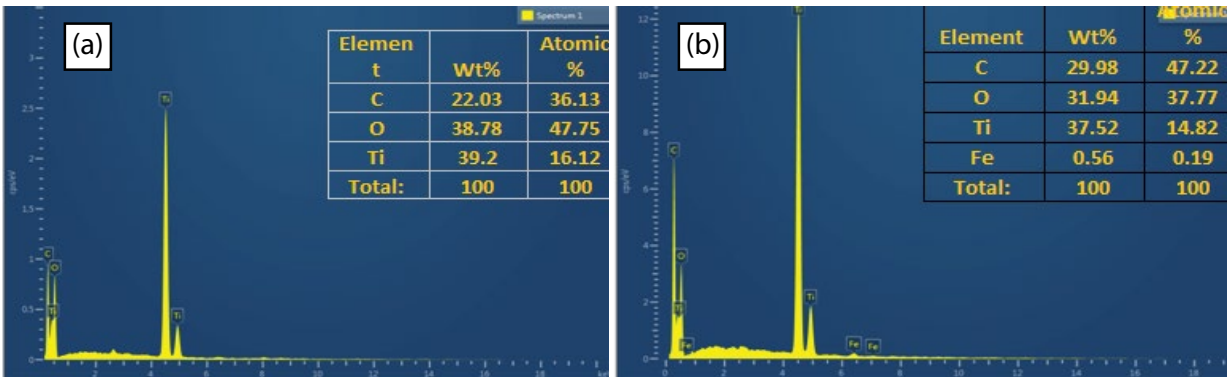

Fig. 6. EDAX model of PNT nanocomposite before (a) and after (b) elimination of dyes.

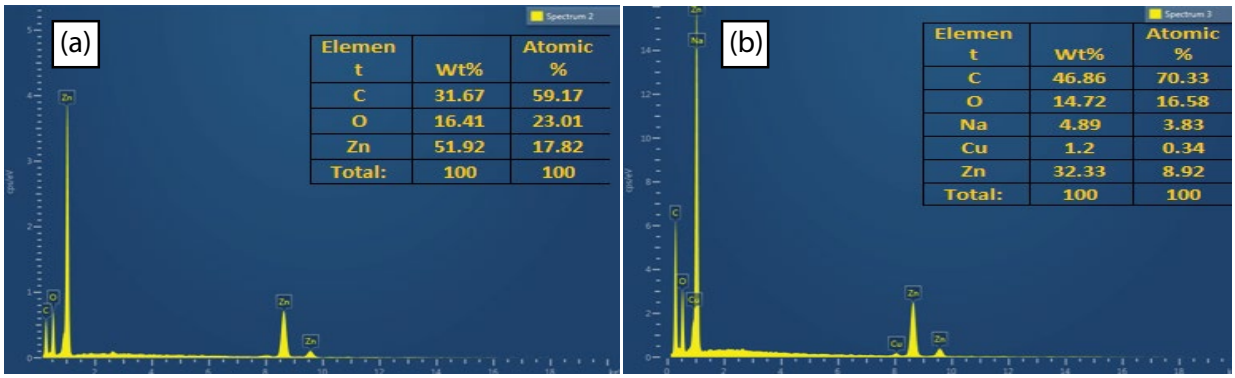

Fig. 7. EDAX model of PNZ nanocomposite before (a) and after (b) elimination of dyes.

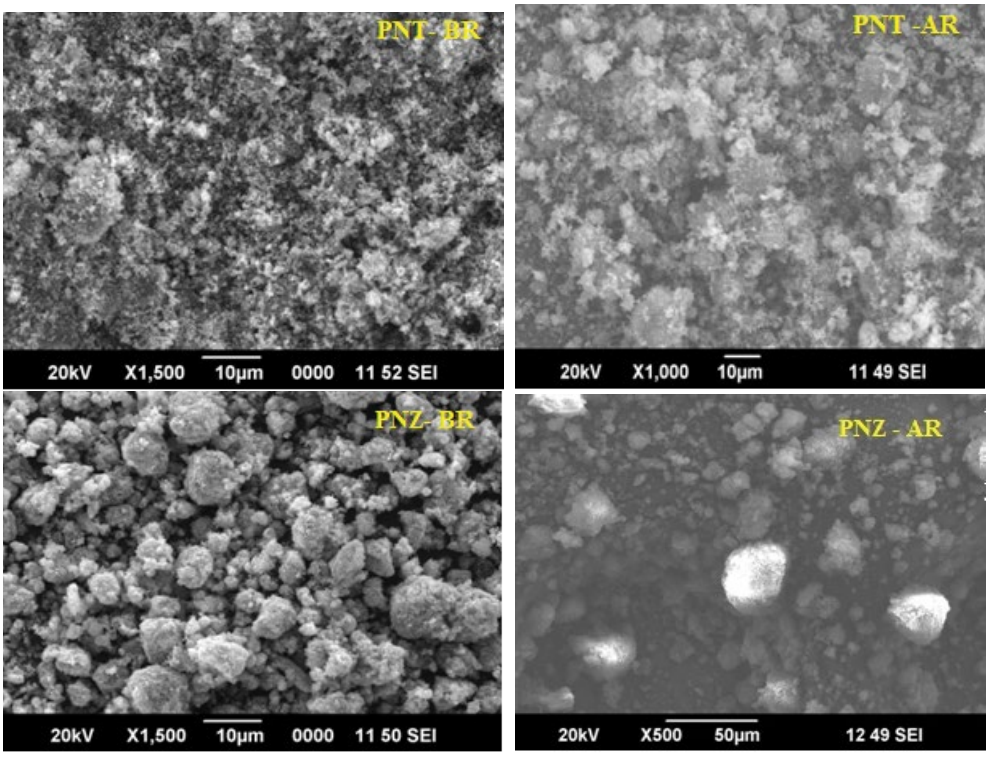

Fig. 8. Scanning electron microscope image of PNT and PNZ nanocomposite before (BR) and after (AR) elimination of dyes.

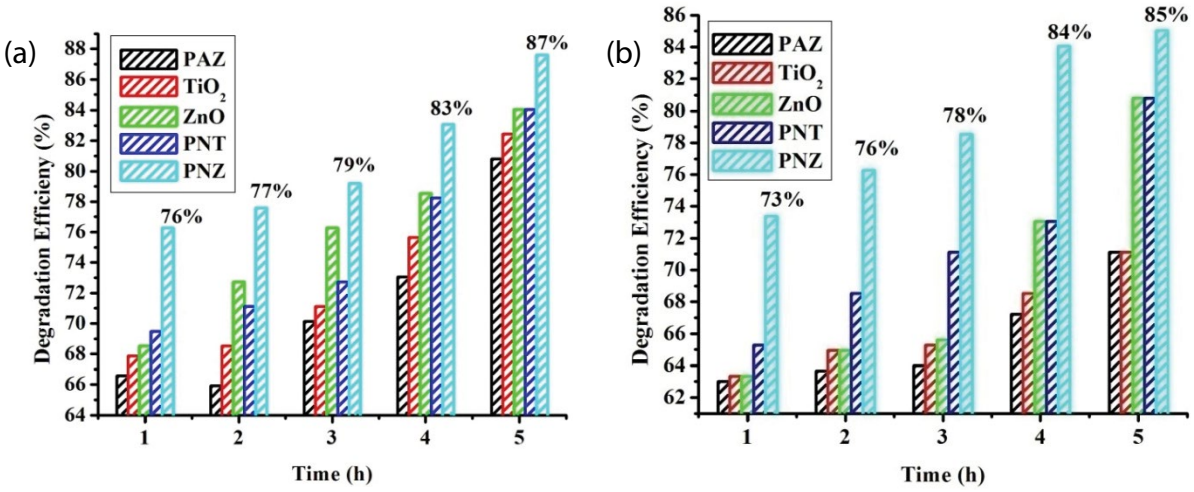

Fig. 9. Deprivation efficacy of MO dye in natural sunlight irradiation with 100 mg catalyst PAZ, ZnO, TiO_2, PNT and PNZ at 10 ppm (a) and 20 ppm (b) dye concentration.

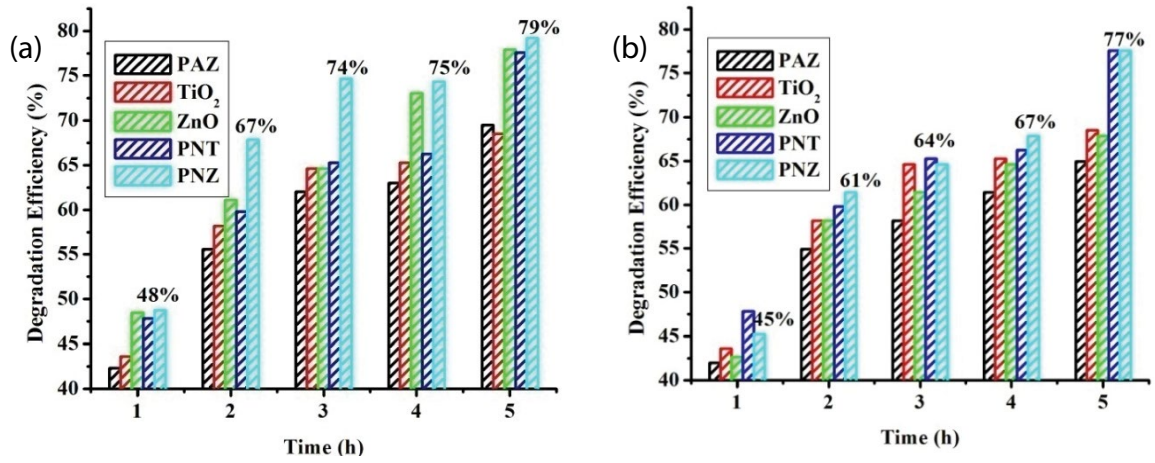

Fig. 10. Deprivation efficacy of MO dye in natural sunlight irradiation with 100 mg catalyst PAZ, ZnO, TiO_2, PNT and PNZ at 30 ppm (a) and 40 ppm (b) dye concentration.

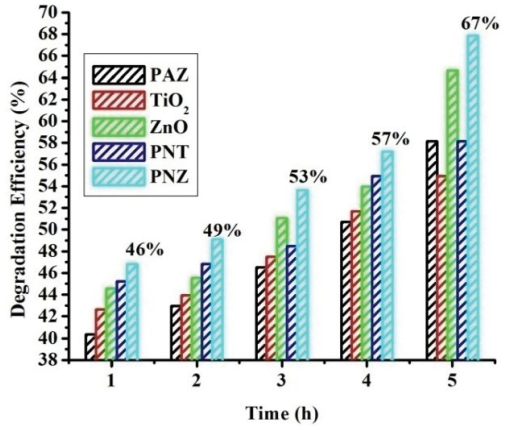

Fig. 11. Deprivation efficacy of MO dye in natural sunlight irradiation with 100 mg catalyst PAZ, ZnO, TiO_2, PNT and PNZ at 50 ppm dye concentration.

intensity of UV light in stimulated remains constant throughout the experiment because it is highly focused, so the maximum degradation efficiency >90% was obtained using stimulated UV-Visible radiation and stimulated solar radiation, whereas the intensity of natural sunlight may vary due to weather conditions.

3.3. Kinetic studies

The kinetics, rate of degradation efficiency of MO, ARS and the mechanism of photocatalytic process of these morphologies of PAZ, PNT, PNZ, TiO_2 and ZnO was studied. It also gives the factors that affect the speeds of a chemical reaction. Chemical kinetics study elucidates detailed observations of the experimental conditions that influence the rate of a chemical reaction and aid in the attainment of equilibrium in a reasonable time [38].

The kinetics of the photodegradation process was explored using two kinetic models, pseudo-first-order

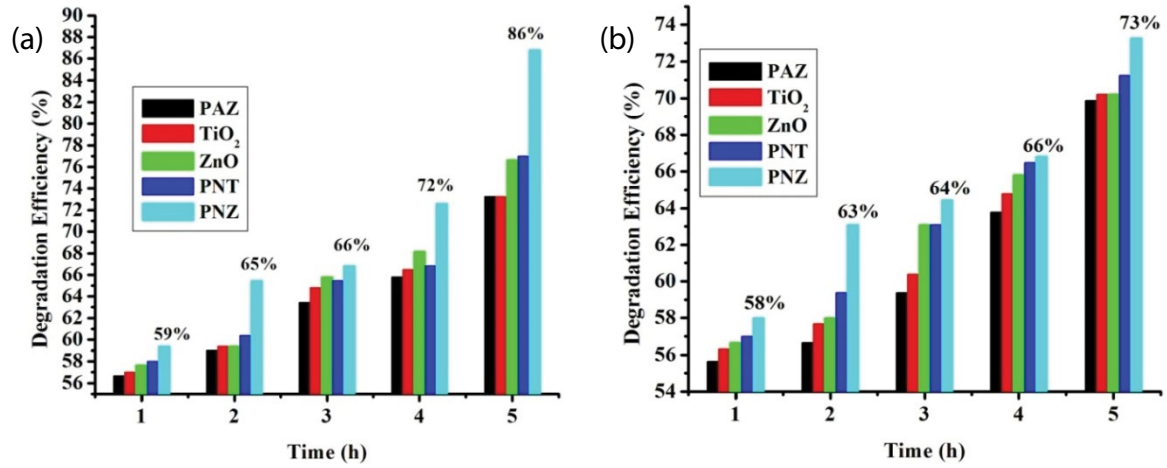

Fig. 12. Deprivation efficacy of ARS dye in natural sunlight irradiation with 100 mg catalyst PAZ, ZnO, TiO_2, PNT and PNZ at 10 ppm (a) and 20 ppm (b) dye concentration.

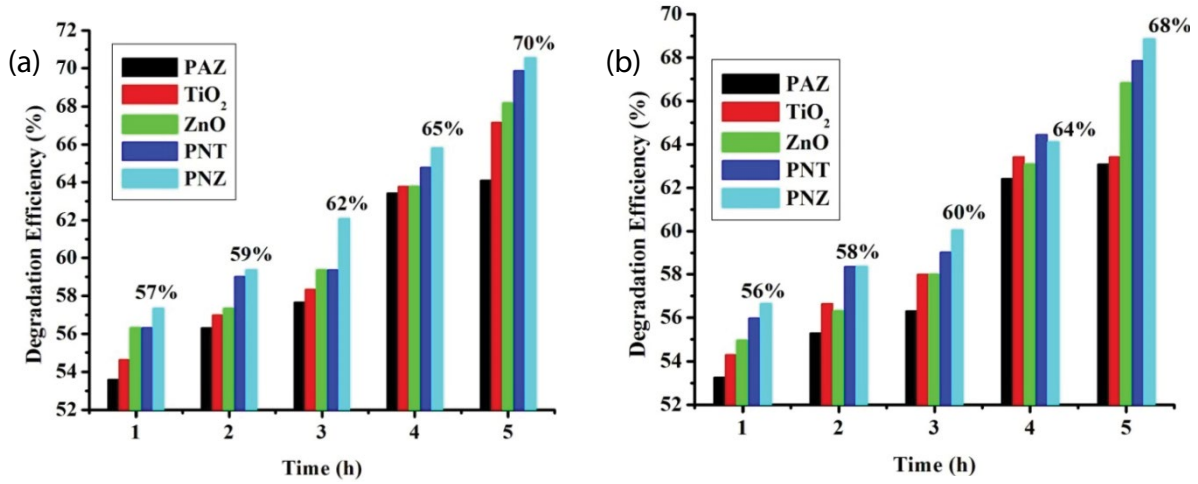

Fig. 13. Deprivation efficacy of ARS dye in natural sunlight irradiation with 100 mg catalyst PAZ, ZnO, TiO_2, PNT and PNZ at 30 ppm (a) and 40 ppm (b) dye concentration.

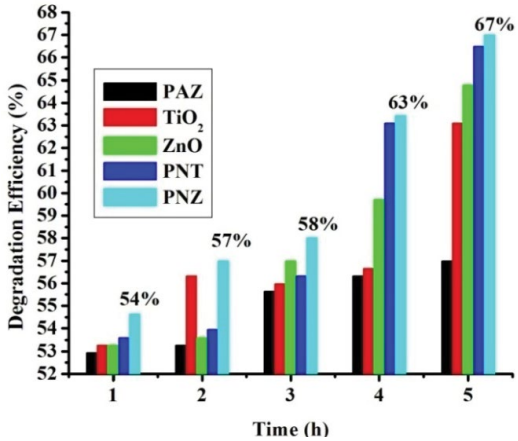

Fig. 14. Deprivation efficacy of ARS dye in natural sunlight irradiation with 100 mg catalyst PAZ, ZnO, TiO_2, PNT and PNZ at 50 ppm dye concentration.

and pseudo-second-order, because photocatalytic process is considered as important in heterogeneous conditions. These models elucidated in the following section.

3.3.1. Pseudo-first-order kinetic model

The pseudo-first-order kinetic equation:

$$\ln\frac{C_0}{C_t} = Kt + C \tag{3}$$

where C_0 is initial concentration of MO and ARS, C_t is the concentration of dyes at a different contact time t, K is the pseudo-first-order rate constant (min^{-1}).

The pseudo-second-order kinetic model is:

$$\frac{t}{q_t} = \frac{1}{K_2 q_e} + \frac{t}{q_e} \tag{4}$$

Table 7
Maximum degradation of photocatalysts

Dosage: 100 mg, 10 ppm, contact time: 5 h					
	PAZ	TiO_2	ZnO	PNT	PNZ
Methyl orange degradation efficiency (%)					
10 ppm	80.82	80.44	81.06	81.06	87.00
20 ppm	71.11	71.11	80.82	80.82	85.03
30 ppm	69.49	68.52	77.91	77.58	79.20
40 ppm	64.96	68.52	67.87	77.58	77.58
50 ppm	58.17	54.93	64.64	58.17	67.07
Alizarin Red S degradation efficiency (%)					
10 ppm	73.27	73.27	76.66	77.00	86.31
20 ppm	69.88	70.22	70.22	71.24	73.27
30 ppm	64.12	67.17	68.19	69.88	70.56
40 ppm	63.10	63.44	66.83	67.85	68.86
50 ppm	57.00	63.10	64.80	66.49	67.00

where q_t is the amount of dye removal at time t, q_e is the amount of dye removal at equilibrium, K is the pseudo-second-order rate constant (min^{-1}).

A straight line plot of $\ln C_0/C_t$ vs. time for pseudo-first-order reaction and t/q_t vs. time for pseudo-second-order reaction using photocatalysts (PAZ, PNT, PNZ, TiO, and ZnO) is shown in Figs. 15–24.

On evaluating the pseudo-first-order and second-order models from Table 8 and Figs. 15–24, comparing the R-values, it is obvious that the pseudo-first-order model was applicable to the process and that the pseudo-second-order model was not applicable to the kinetics of the degradation process [21]. From the results, pseudo-first-order fits the process better than pseudo-second-order.

3.3.2. Langmuir isotherm

The Langmuir isotherm model was used to determine the best adsorption ability assuming 100% monolayer coverage on the adsorbent surface [27].

Langmuir equation is commonly expressed as follows:

$$\frac{C_e}{q_e} = \frac{1}{q_m C_e} + \frac{1}{K_a q_m} \tag{5}$$

where C_e is the dye concentration in solution at equilibrium, q_e is the unit equilibrium adsorption capacity, q_m is the maximum dye uptake, and K_a is a constant denoting the energy of adsorption and affinity of the binding sites providing information on adsorption capacity throughout a monolayer.

By plotting C_e/q_e vs. C_e values of q_m and K_a can be calculated (Fig. 25).

A non-dimension constant separation factor or equilibrium parameter R_L, can express the crucial uniqueness of a Langmuir isotherm which is given by:

$$R_L = \frac{1}{\left(1 + K_L C_e\right)} \tag{6}$$

The influence of isotherm shape on favorable or unfavorable photocatalytic process has been considered. The R_L rate specify that whether the type of the isotherm were unfavorable ($R_L > 1$), linear ($R_L = 1$), favorable ($0 < R_L < 1$) or irreversible ($R_L = 0$). In the present experiment results which were mentioned in the Table 9 were found for R_L between 0.892 and 0.987 which clearly indicate the photocatalytic process was favorable [29].

3.3.3. Freundlich isotherm

The Freundlich equation was demonstrated for the elimination of dyes MO and ARS on the catalyst. The Freundlich isotherm was represented by:

$$\log q_e = \log K_f + \frac{1}{n} \log C_e \tag{7}$$

where q_e represents the amount of dye removed, C_e represents the solution's equilibrium concentration, and K_f and

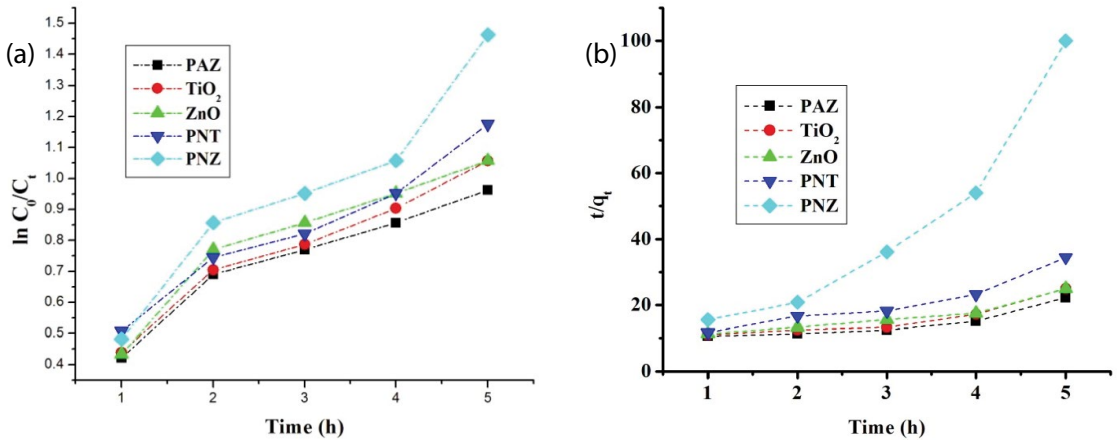

Fig. 15. Pseudo-first-order (a) and pseudo-second-order (b) kinetics model of decolourization for 10 ppm MO dye using 100 mg catalysts (PAZ, ZnO, TiO_2, PNT and PNZ).

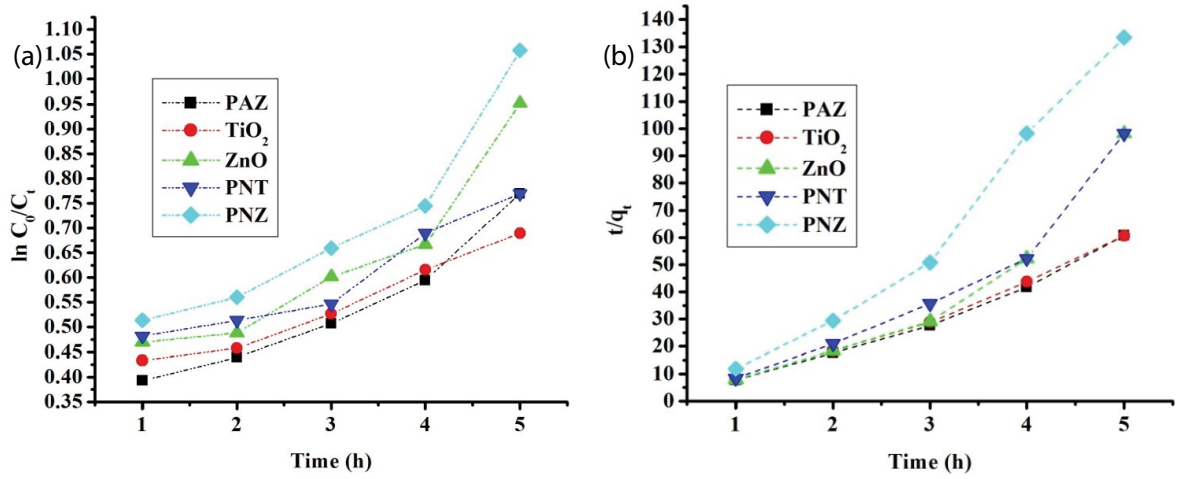

Fig. 16. Pseudo-first-order (a) and pseudo-second-order (b) kinetics model of decolourization for 20 ppm MO dye using 100 mg catalysts (PAZ, ZnO, TiO_2, PNT and PNZ).

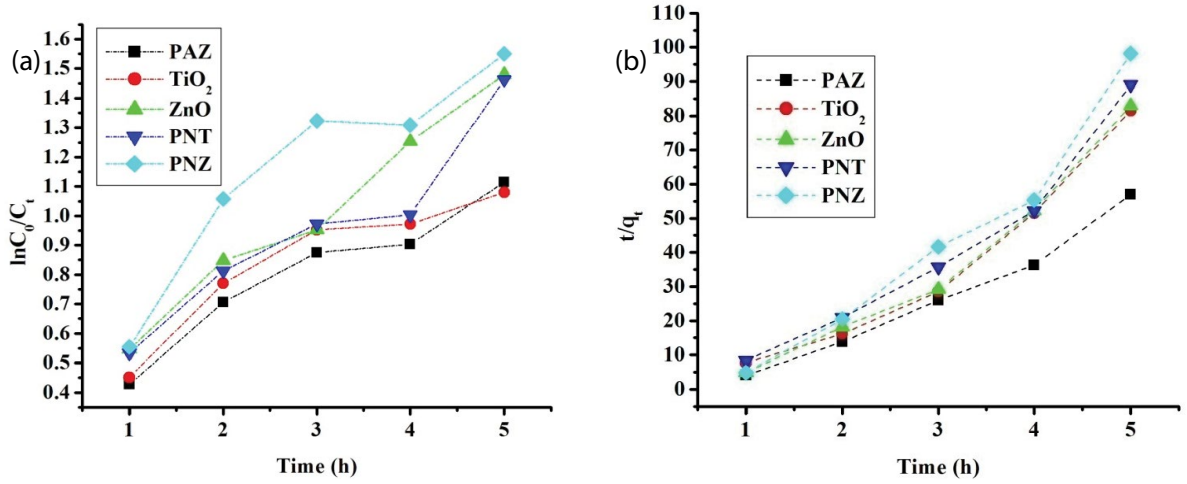

Fig. 17. Pseudo-first-order (a) and pseudo-second-order (b) kinetics model of decolourization for 30 ppm MO dye using 100 mg catalysts (PAZ, ZnO, TiO_2, PNT and PNZ).

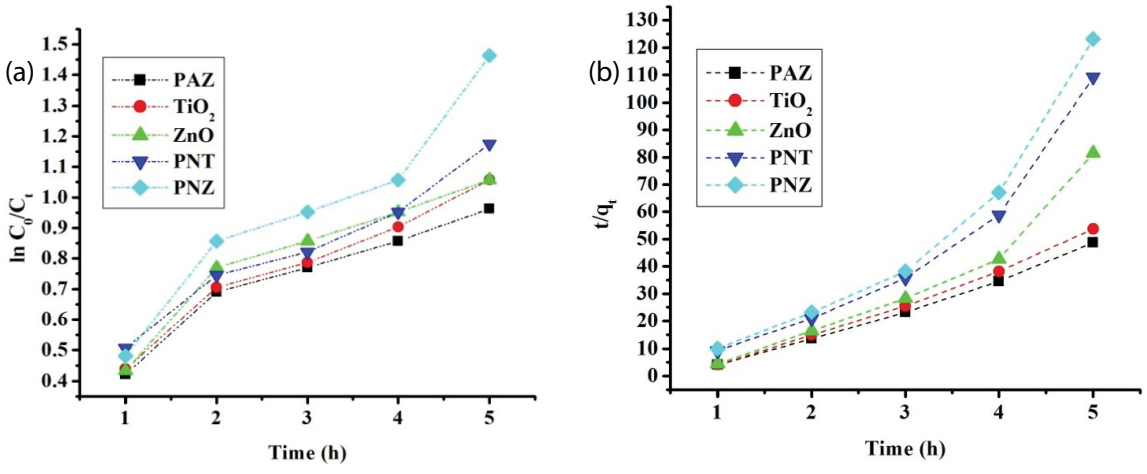

Fig. 18. Pseudo-first-order (a) and pseudo-second-order (b) kinetics model of decolourization for 40 ppm MO dye using 100 mg catalysts (PAZ, ZnO, TiO_2, PNT and PNZ).

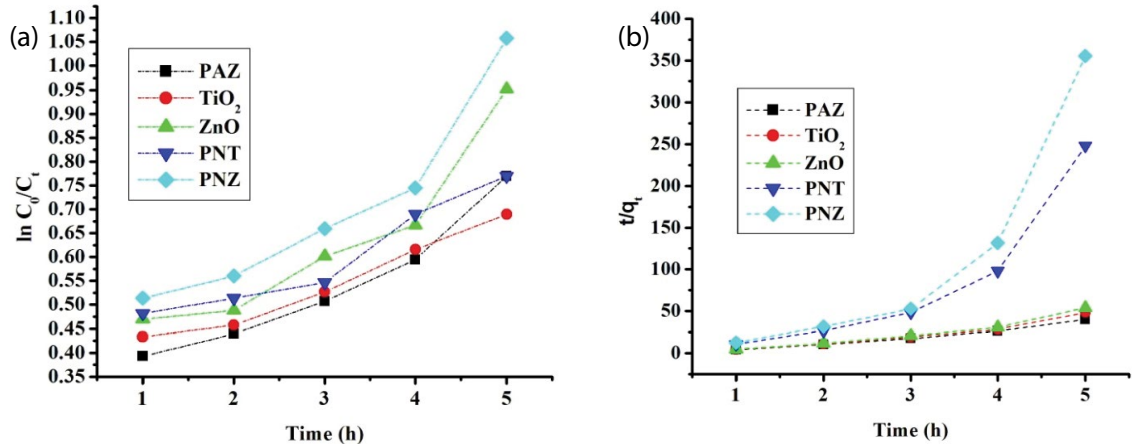

Fig. 19. Pseudo-first-order (a) and pseudo-second-order (b) kinetics model of decolourization for 50 ppm MO dye using 100 mg catalysts (PAZ, ZnO, TiO_2, PNT and PNZ).

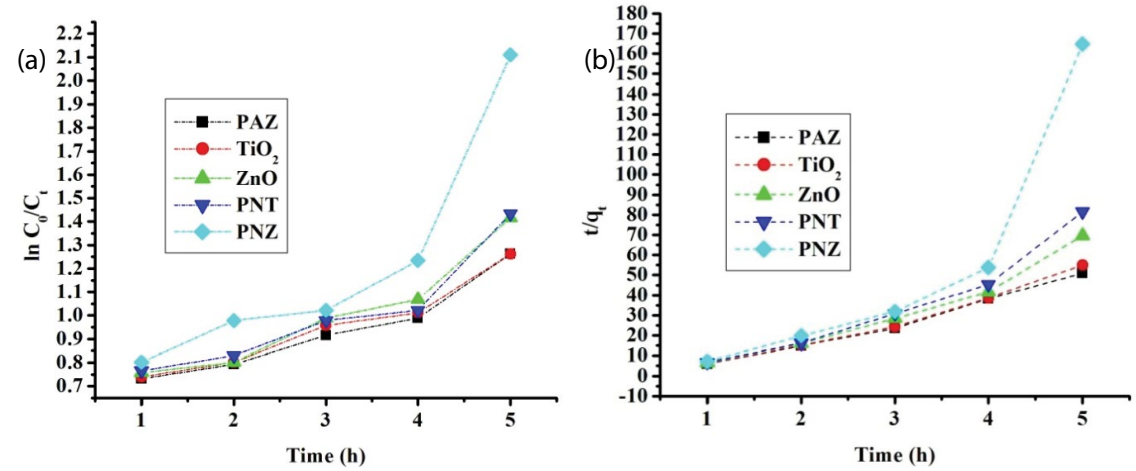

Fig. 20. Pseudo-first-order (a) and pseudo-second-order (b) kinetics model of decolourization for 10 ppm ARS dye using 100 mg catalysts (PAZ, ZnO, TiO_2, PNT and PNZ).

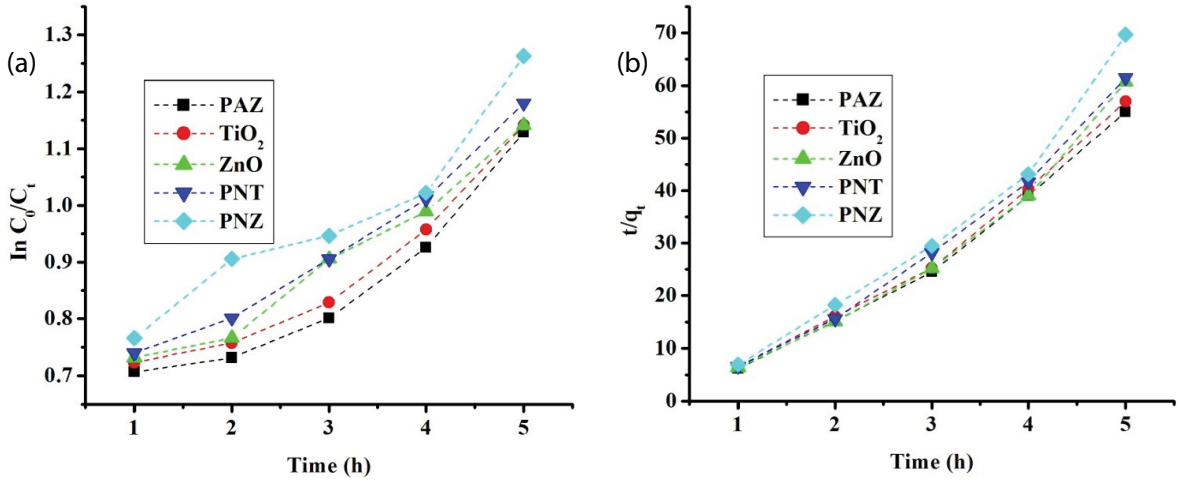

Fig. 21. Pseudo-first-order (a) and pseudo-second-order (b) kinetics model of decolourization for 20 ppm ARS dye using 100 mg catalysts (PAZ, ZnO, TiO_2, PNT and PNZ).

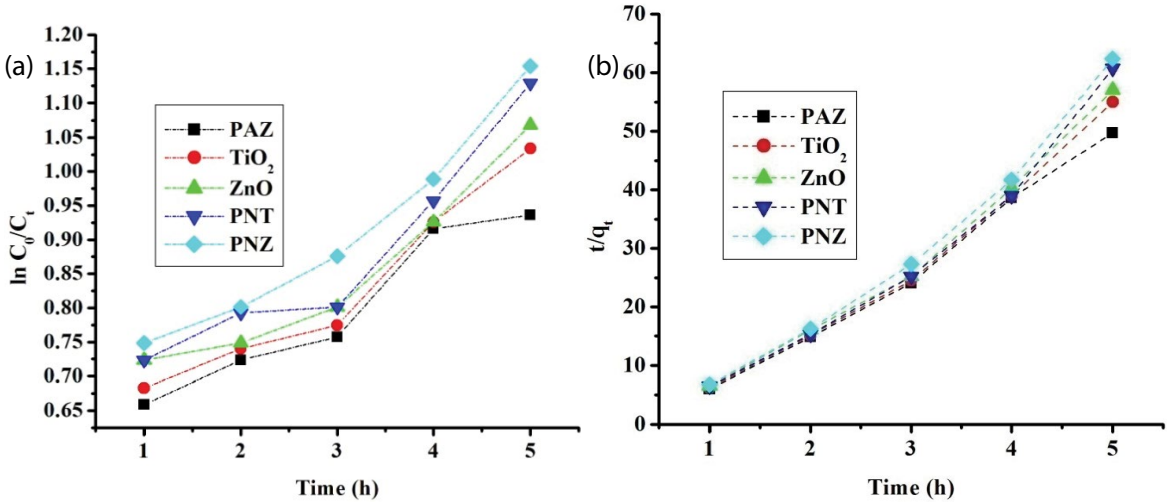

Fig. 22. Pseudo-first-order (a) and pseudo-second-order (b) kinetics model of decolourization for 30 ppm ARS dye using 100 mg catalysts (PAZ, ZnO, TiO_2, PNT and PNZ).

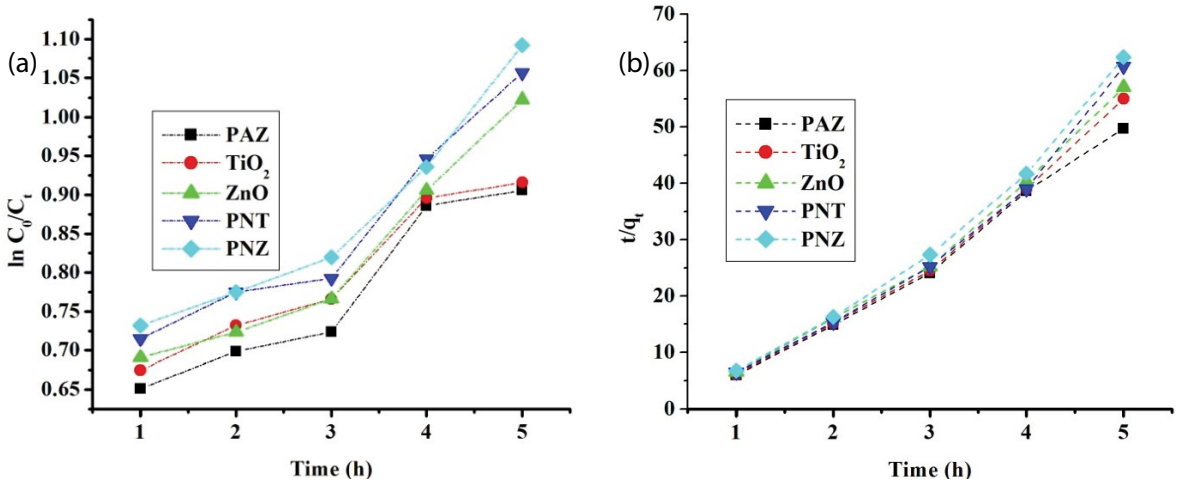

Fig. 23. Pseudo-first-order (a) and pseudo-second-order (b) kinetics model of decolourization for 40 ppm ARS dye using 100 mg catalysts (PAZ, ZnO, TiO_2, PNT and PNZ).

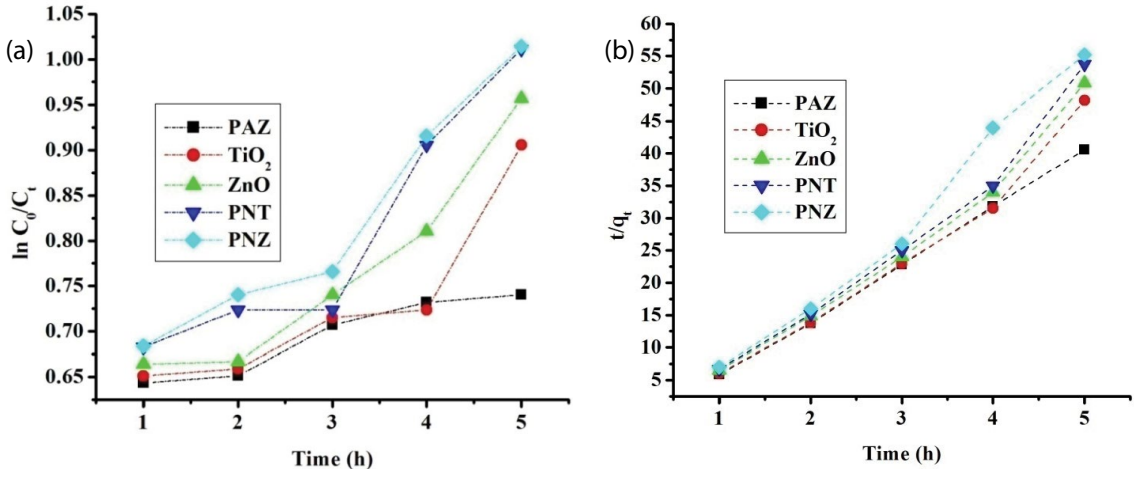

Fig. 24. Pseudo-first-order (a) and pseudo-second-order (b) kinetics model of decolourization for 50 ppm ARS dye using 100 mg catalysts (PAZ, ZnO, TiO_2, PNT and PNZ).

Table 8
Kinetic model results for degradation of anionic dyes using photocatalysts

	Methyl orange						Alizarin Red S					
	Pseudo-first-order			Pseudo-second-order			Pseudo-first-order			Pseudo-second-order		
Dye variation	Intercept	Slope	*r*-value	Intercept	Slope	*r*-value	Intercept	Slope	*r*-value	Intercept	Slope	*r*-value
10 ppm	1.121	0.121	0.993	6.217	2.31	0.904	0.709	0.016	0.995	5.626	0.313	0.92
20 ppm	0.913	0.201	0.998	35.4	18.27	0.895	0.907	0.024	0.969	50.67	3.368	0.899
30ppm	0.402	0.033	0.911	12.54	1.792	0.914	0.698	0.02	0.989	47.73	3.079	0.91
40 ppm	0.809	0.045	0.991	21.94	20.45	0.916	0.632	0.02	0.995	44.78	0.142	0.942
50 ppm	0.549	0.037	0.977	0.193	2.347	0.841	0.631	0.011	0.968	5.551	0.289	0.915

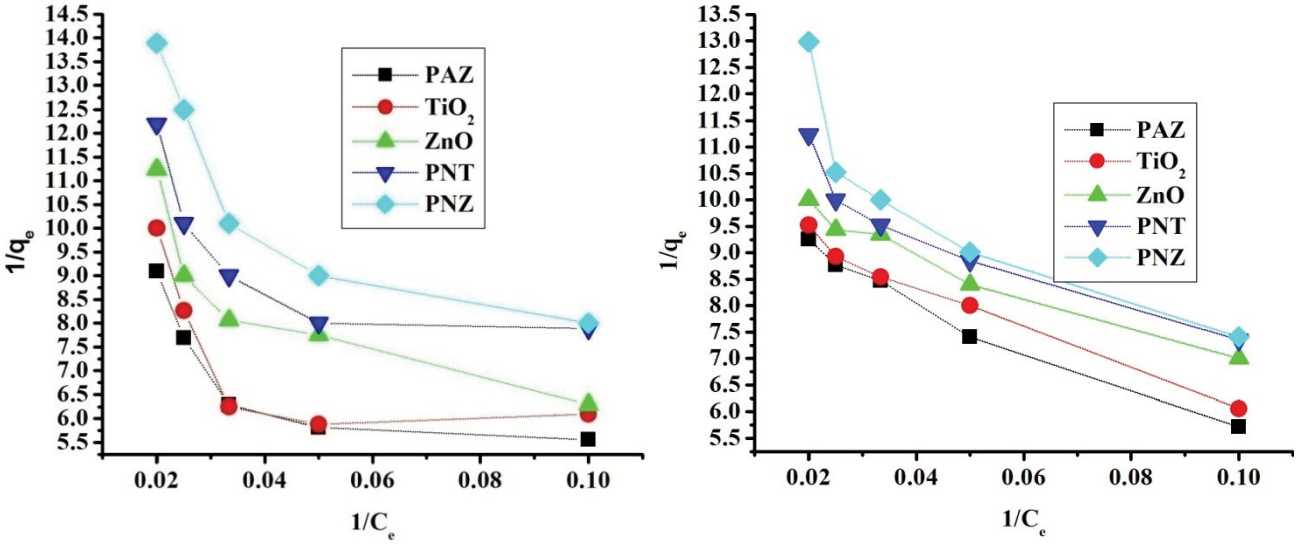

Fig. 25. Langmuir isotherm for the removal of MO and ARS by catalyst PAZ, ZnO, TiO_2, PNZ and PNT.

Table 9
Langmuir isotherm values of intercept and slope in the removal of anionic dyes using photocatalysts

	Langmuir isotherm					
	Methyl orange			Alizarin Red S		
Dye variation	Intercept	Slope	*r*-value	Intercept	Slope	*r*-value
10 ppm	6.076	1.145	0.91	7.969	0.402	0.945
20 ppm	7.744	1.179	0.987	7.85	0.916	0.892
30 ppm	4.762	0.668	0.906	8.158	0.458	0.971
40 ppm	4.742	0.849	0.923	7.117	0.405	0.968
50 ppm	4.828	1.037	0.944	5.303	0.406	0.913

Table 10
Freundlich isotherm values of intercept and slope in the removal of anionic dyes using photocatalysts

	Freundlich isotherm					
	Methyl orange			Alizarin Red S		
Dye variation	K_f	*n*	*r*-value	K_f	*n*	*r*-value
10 ppm	–0.799	–0.008	0.553	–0.915	–0.02	0.976
20 ppm	–0.888	–0.029	0.561	–0.904	–0.019	0.942
30 ppm	–0.945	–0.031	0.728	–0.742	–0.03	0.61
40 ppm	–0.992	–0.03	0.728	–0.857	–0.021	0.92
50 ppm	–0.888	–0.029	0.561	–0.912	–0.036	0.915

n represent the elements that change the adsorption capacity and intensity, respectively. The degradation of dyes follows the Freundlich adsorption isotherm, as shown by linear graphs of $\log q_e$ vs. $\log C_e$ in Table 10 and Fig. 26.

The values of K_f and n in Table 10 reveal that as negative charges on the photocatalyst surface build, an electrostatic force similar to the van der waals force develops between the catalyst surface and the dye. If *n* is equal to unity, the photocatalytic process is linear; if *n* is less than unity, the photocatalytic process is chemical; and if *n* is greater than unity, the photocatalytic process is favourable. From the Table 10, it was found that the degradation process is

favorable. The intensity of adsorption is determined by the *n* value, which reflects the bond energies between dye and photocatalysts as well as the probability of minimal chemisorptions occurs rather than physisorption [37].

3.4. Mechanism of photocatalysts

The photocatalytic oxidation mechanism (Fig. 27) using semiconducting materials can be summarized as follows;

- *Photoexcitation*: When a photoelectron is promoted from the filled valence band of a semiconductor photocatalyst, such as TiO_2, to the empty conduction band as a result of irradiation, a photocatalytic reaction is activated. The energy (hv) of the absorbed photon is equal to or greater than the band gap of the semiconductor photocatalyst [38]. The valence band (h^+_{VB}) is left with a hole due to the excitation process. As a result, an electron and hole pair (e/h^+) is created, as shown in the equation below.
- *Ionization of water*: The photogenerated holes at the valence band then react with water to produce $OH^\bullet$ radical.

The $HO^\bullet$ radical formed on the irradiated semiconductor surface are very dominant oxidizing agent. It attacks

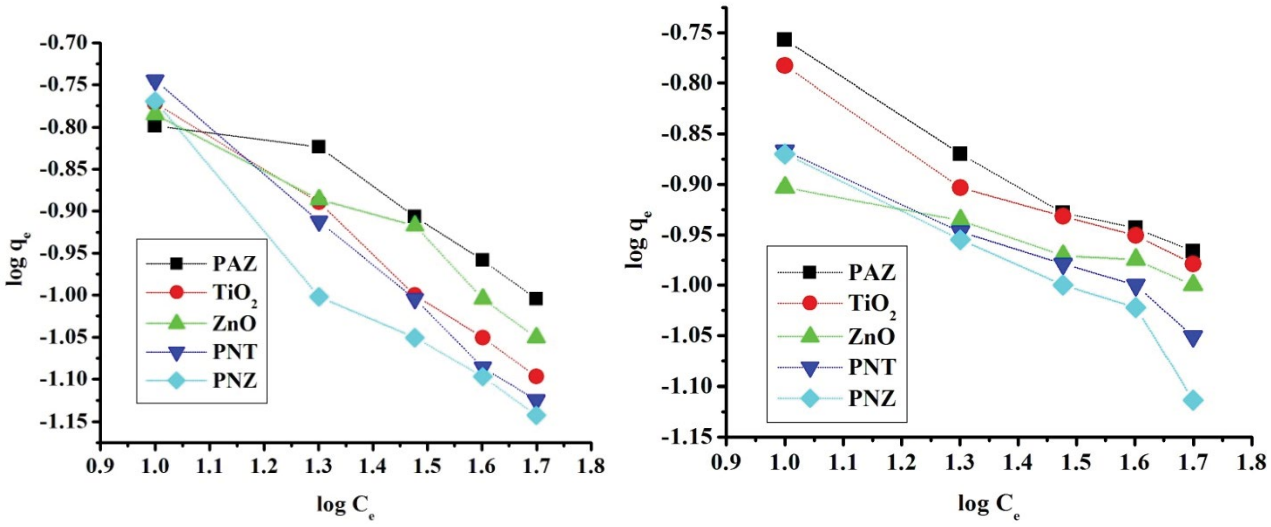

Fig. 26. Freundlich isotherm for the removal of MO and ARS by catalyst PAZ, ZnO, TiO_2, PNZ and PNT.

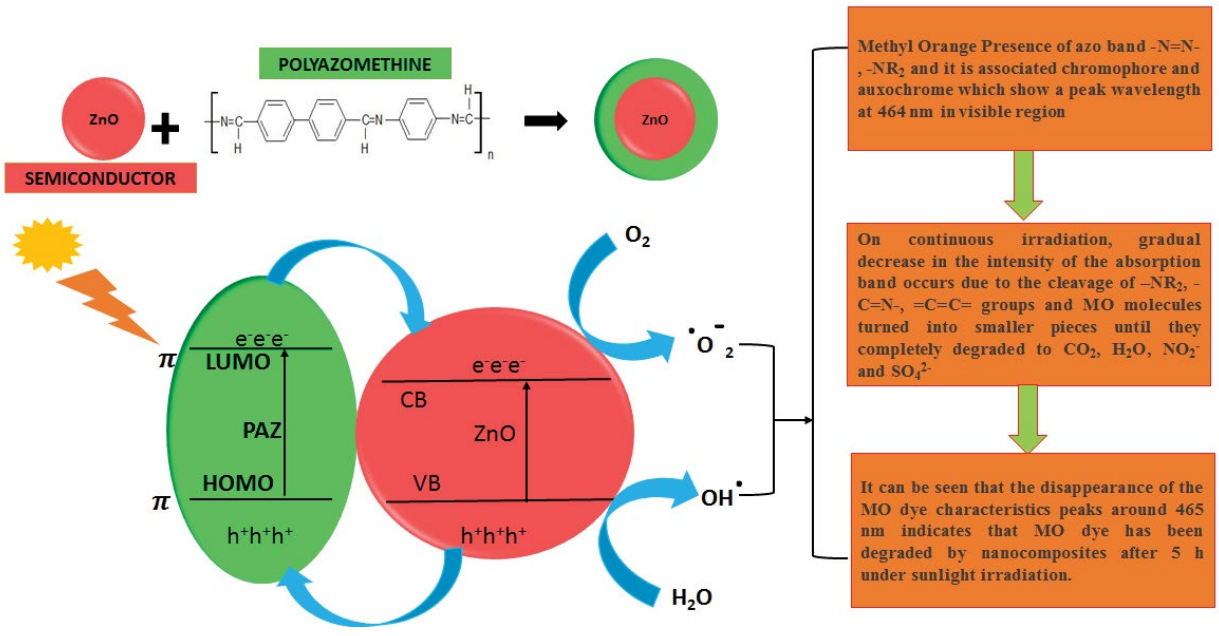

Fig. 27. Photocatalyst mechanism of methyl orange (MO) degradation.

adsorbed organic molecules or those that are very close to the catalyst surface non-selectively, producing them to mineralize to a level based on their structure and steadiness level. It does not only easily attack organic contaminants but can also attack microorganisms for their higher decontamination.

- *Oxygenionosorption*: While the photogenerated hole (h^+_{VB}) reacts with surface bound water or OH^- to produce the hydroxyl radical, electron in the conduction (e^-_{CB}) is taken up by the oxygen in order to generate anionic superoxide radical (O_2^-).

This superoxide ion may not only take part in the further oxidation process but also avoids the electron-hole recombination, thus maintaining electron neutrality within the TiO_2 molecule [39].

- *Protonation of superoxide*: The superoxide ($O_2^{-\bullet}$) produced gets protonated forming hydroperoxyl radical ($HO_2^\bullet$) and then consequently H_2O_2 which further separates into highly reactive hydroxyl radicals ($OH^\bullet$).

Both oxidation and reduction processes commonly take place on the surface of the photoexcited semiconductor photocatalyst.

Therefore a semiconductor photocatalyst can take part in a redox reaction upon photo-excitation on its surface effectively. The general scheme of a photocatalytic reaction involving a semiconductor material used for the dye degradation [Eqs. (8)–(14)]:

$$\text{Dye} + h\nu \rightarrow \text{Dye}^* \quad (8)$$

$$\text{Dye}^* + TiO_2 \rightarrow \text{Dye}^{\bullet+} + TiO_2 \quad (9)$$

$$TiO_{2(e)} + O_2 \rightarrow TiO_2 + O_2^- \quad (10)$$

$$O_2^- + TiO_{2(e)} + 2H^+ \rightarrow H_2O_2 \quad (11)$$

$$H_2O_2 + TiO_{2(e)} \rightarrow OH^\bullet + OH^- \quad (12)$$

$$\text{Dye}^{\bullet+} + O_2\left(O_2^- \text{ or } OH^-\right) \rightarrow \text{Organic intermediates} \quad (13)$$

$$\text{Organic intermediates} \rightarrow \text{Degraded or mineralized products} \quad (14)$$

4. Conclusion

The photocatalytic removal of dye pollution from textile waste water by PAZ, PNT, PNZ, TiO_2, and ZnO nanocomposites in the presence of natural sunlight was examined in this study. The effects of dye variation were investigated. The effectiveness of MO and ARS degradation reduces as the initial concentration of the dyes increase. In the dye variation investigation, the maximum degradation efficiency was 86% and 87% in the presence of natural sunlight and the optimum dye concentration was 10 ppm at 100 mg photocatalyst dosage.

PAZ, PNT, PNZ, TiO_2, and ZnO nanocomposites were used as a catalyst in the presence of natural sunlight to study kinetic isotherm pseudo-first-order and pseudo-second-order for dye variation. The best fit model was found to be pseudo-first-order based on the graph *r*-value. Adsorption isotherm Langmuir and Freundlich has been analyzed for dye variation parameter in the removal of anionic dyes (MO and ARS). Graphs have been plotted for each isotherm and intercept, slope, *r*-value was obtained from them. From the two isotherm model it was found that Langmuir is the best fit model and from Freundlich it was found that slight chemisorptions process was carried out.

Acknowledgement

The authors express their gratitude to the Hindusthan College of Engineering and Technology management and principal for their assistance in completing the project successfully.

References

[1] U. Riaz, S.M. Ashraf, J. Kashyap, Role of conducting polymers in enhancing TiO_2-based photocatalytic dye degradation: a short review, Polym. Plast. Technol. Eng., 54 (2015) 1850–1870.
[2] T.-J. Whang, M.-Tao Hsieh, H.-H. Chen, Visible-light photocatalytic degradation of methylene blue with laser-induced Ag/ZnO nanoparticles, Appl. Surf. Sci., 258 (2012) 2796–2801.
[3] N.A. Jumat, P.S. Wai, J.J. Ching, W.J. Basirun, Synthesis of polyaniline-TiO_2 nanocomposites and their application in photocatalytic degradation, Polym. Polym. Compos., 25 (2017) 507–513.
[4] A. Esrafil, A. Esrafili, J.J. Ahmad, R.K. Roshanak, F. Mahdi, Synthesis of TiO_2/polyaniline photocatalytic nanocomposite and its effects on degradation of metronidazole in aqueous solutions under UV and visible light radiation, Desal. Water Treat., 161 (2019) 228–242.
[5] Q. Tang, J. Lin, Z. Wu, J. Wu, M. Huang, Y. Yang, Preparation and photocatalytic degradability of TiO_2/polyacrylamide composite, Eur. Polym. J., 43 (2007) 2214–2220.
[6] Y. Zhu, Y. Dan, Photocatalytic activity of poly(3-hexylthiophene)/titanium dioxide composites for degrading methyl orange, Sol. Energy Mater. Sol. Cells, 94 (2010) 1658–1664.
[7] Y. Zhu, S. Xu, L. Jiang, K. Pan, Y. Dan, Synthesis and characterization of polythiophene/titanium dioxide composites, React. Funct. Polym., 68 (2008) 1492–1498.
[8] V. Eskizeybek, F. Sarı, H. Gülce, A. Gülce, A. Avcı, Preparation of the new polyaniline/ZnO nanocomposite and its photocatalytic activity for degradation of methylene blue and malachite green dyes under UV and natural sun lights irradiations, Appl. Catal., B, 119– 120 (2012) 197–206.
[9] Y.-G. Peng, J.-L. Ji, Y.-L. Zhang, H.-X. Wan, D.-J. Chen, Preparation of poly(*m*-phenylenediamine)/ZnO composites and their photocatalytic activities for degradation of C.I. Acid red 249 under UV and visible light irradiations, Environ. Prog. Sustainable Energy, 33 (2014) 123–130.
[10] H. Gülce, V. Eskizeybek, B. Haspulat, F. Sarı, A. Gülce, A. Avcı, Preparation of a new polyaniline/CdO nanocomposite and investigation of its photocatalytic activity: comparative study under UV light and natural sunlight irradiation, Ind. Eng. Chem. Res., 52 (2013) 10924–10934.

[11] J. Ruxangul, O. Yakupjan, R. Adalet, A. Ahmat, Z. Yu, A. Tursun, Solid-state synthesis and photocatalytic activity of polyterthiophene derivatives/TiO_2 nanocomposites, Materials, 7 (2014) 3786–3801.
[12] A. Tursun, A. Ahmat, J. Ruxangul, O. Yakupjan, Z. Yu, A facile solid-state heating method for preparation of poly(3,4-ethelenedioxythiophene)/ZnO nanocomposite and photocatalytic activity, Nano Res. Lett., 9 (2014) 89, doi: 10.1186/1556-276X-9-89.
[13] Z. Katancic, S. Suka, K. Vrbat, A. Tasic, Z. Murgic, Synthesis of PEDOT/ZnO photocatalyst: validation of photocatalytic activity by degradation of Azo RR45 dye under solar and UV-A irradiation, Chem. Biochem. Eng., 31 (2017) 385–394.
[14] M.O. Ansari, M.M. Khan, S.A. Ansari, M.H. Cho, Polythiophene nanocomposites for photodegradation applications: past, present and future, J. Saudi Chem. Soc., 19 (2015) 494–504.
[15] S. Shahabuddin, M.S. Norazilawati, M. Sharifah, J.C. Juan, $SrTiO_3$ nanocube-doped polyaniline nanocomposites with enhanced photocatalytic degradation of methylene blue under visible light, Polymers, 8 (2016) 27, doi: 10.3390/polym8020027.
[16] A.-F. Daniel, S. Jakub, C. Emerson, Recent developments in polydopamine-based photocatalytic nanocomposites for energy production: physico-chemical properties and perspectives, Catal. Today, 397–399 (2022) 316–349.
[17] D. Pathania, D. Gupta, A.H. Al-Muhtaseb, G. Sharma, A. Kumar, Mu. Naushad, T. Ahamad, S.M. Alsehri, Photocatalytic degradation of highly toxic dyes using chitosan-*g*-poly(acrylamide)/ZnS in presence of solar irradiation, J. Photochem. Photobiol., A, 329 (2016) 61–68.
[18] K.K. Melek, S. Munevver, B. Zekeriya, Photocatalytic efficiency of metallo phthalocyanine sensitized TiO_2 (MPc/TiO_2) nanocomposites for Cr(VI) and antibiotic amoxicillin, Water, 13 (2021) 2174, doi: 10.3390/w13162174.
[19] Z. Jannatun, F. Fizzah, R. Ufana, A comprehensive review on the photocatalytic activity of polythiophene-based nanocomposites against degradation of organic pollutants, Catal. Sci. Technol., 11 (2021) 6630–6648.
[20] C. Yang, W. Dong, G. Cui, Y. Zhao, X. Shi, X. Xia, B. Tang, W. Wang, Highly-efficient photocatalytic degradation of methylene blue by PoPD-modified TiO_2 nanocomposites due to photosensitization-synergetic effect of TiO_2 with PoPD, Sci. Rep., 7 (2017) 3973, doi: 10.1038/s41598-017-04398-x.
[21] S. Murugan, M.S. Mariappan, Development of efficiency improved polymer-modified TiO_2 for the photocatalytic degradation of an organic dye from wastewater environment, Appl. Water Sci., 7 (2017) 1781–1790.
[22] A.A. Al-Kahtani, Photocatalytic degradation of Rhodamine B dye in wastewater using gelatin/CuS/PVA nanocomposites under solar light irradiation, J. Biomater. Nanobiotechnol., 8 (2017) 66–82.
[23] C. Dan, W. Weide, Z. Fan, Y. Yan, Q. Guangren, Visible light photocatalytic degradation of methylene blue by $H_2O_2/NiFe_2O_4$ synthesized from wastewater, Desal. Water Treat., 96 (2017) 169–177.
[24] B. Joy Vasanthi, L. Ravikumar, Synthesis and characterization of poly(azomethine ester)s with a pendent dimethoxy benzylidene group, Open J. Polym. Chem., 3 (2013) 1–8, doi: 10.4236/ojpchem.2013.33013.
[25] S.M. Tripathi, D. Tiwari, A. Ray, Electrical conductivity of polyazomethine nanocomposite, Indian J. Chem., 53 (2013) 1505–1512.
[26] S.J. Pradeeba, K. Sampath, A comparative study of photocatalytic degradation efficiency of methylene blue dye in waste water using poly(azomethine)/ZnO nanocomposite and poly(azomethine)/TiO_2 nanocomposite, J. Ovonic Res., 14 (2018) 243–259.
[27] S.J. Pradeeba, K. Sampath, Photodegradation efficiency of methyl orange and Alizarin Red S in waste water using poly(azomethine)/TiO_2 nanocomposite, AIP Conf. Proc., 2162 (2019) 020028.
[28] S.J. Pradeeba, K. Sampath, Synthesis and characterization of poly(azomethine)/ZnO nanocomposite toward photocatalytic degradation of methylene blue, malachite green, and bismarck brown, J. Dyn. Syst. Meas. Control, 141 (2019) 051001, doi: 10.1115/1.4042090.
[29] S.J. Pradeeba, K. Sampath, Degradation of methyl orange and Alizarin Red S from waste water using poly(azomethine)/ZnO nanocomposite as a photocatalyst, AIP Conf. Proc., 2270 (2020) 110001.
[30] S.J. Pradeeba, K. Sampath, K. Kalapriya, Photocatalytic degradation efficiency of malachite green in aqueous medium using poly (azomethine)/ZnOnanocomposite, AIP Conf. Proc., 2142 (2020) 150003.
[31] S.J. Pradeeba, K. Sampath, A. Ramadevi, Photo-catalytic degradations of methylene blue, malachite green and Bismarck brown using poly(azomethine)/TiO_2 nanocomposite, Cluster Comput., 1 (2018) 3893–3909.
[32] S. Krishnan, S.J. Pradeeba, A. Karunakaran, K. Kumarasamy, M.-C. Lin, The effect of pH on the photocatalytic degradation of cationic and anionic dyes using polyazomethine/ZnO and polyazomethine/TiO_2 nanocomposites, Int. J. Appl. Sci. Eng., 18 (2021) 1–8.
[33] S.P. Kim, M.Y. Choi, H.M. Choia, Photocatalytic activity of SnO_2 nanoparticles in methylene blue degradation, Mater. Res. Bull., 74 (2016) 85–89.
[34] S.K. Moosvi, K. Majid, T. Ara, Studying the electrical, thermal, and photocatalytic activity of nanocomposite of polypyrrole with the photoadduct of $K_3[Fe(CN)_6]$ and diethylenetriamine, Mater. Res., 2 (2016) 1–8, doi: 10.1590/1980-5373-MR-2015-0786.
[35] S. Wahyuni, E.S. Kunarti, R.T. Swasono, I. Kartini, Characterization and photocatalytic activity of TiO_2(rod)-SiO_2-polyaniline nanocomposite, Indonesian J. Chem., 18 (2018) 321–330.
[36] D. Wu, F. Wang, Y. Tan, L. Caolong, Facile synthesis of NiS/CdS nanocomposites for photocatalytic degradation of quinoline under visible-light irradiation, RSC Adv., 6 (2016) 73522–73526.
[37] L. Yong, G. Zhanqi, J. Yuefei, H. Xiaobin, S. Cheng, Y. Shaogui, W. Lianhong, W. Qingeng, D. Fang, Photodegradation of malachite green under simulated and natural irradiation: kinetics, products, and pathways, J. Hazard. Mater., 285 (2015) 127–136.
[38] S.P. Patil, V.K. Mahajan, V.S. Shrivastavaa, G.H. Sonawane, Kinetics of photocatalytic degradation of methylene blue by ZnO-bentonite nanocomposite, Iran. Chem. Commun., 5 (2017) 417–428.
[39] E. Perju, L. Ghimpu, G. Hitruc, V. Harabagiu, M. Bruma, L. Marin, Organic–inorganic hybrid nanomaterials based on inorganic oxides and a mesomorphic polyazomethine, High Perform. Polym., 27 (2015) 546–554.